Communication

Ru-Doped Single Walled Carbon Nanotubes as Sensors for SO₂ and H₂S Detection

Navaratnarajah Kuganathan [1,2,*] and **Alexander Chroneos** [1,2]

1   Department of Materials, Imperial College London, London SW7 2AZ, UK;
    alexander.chroneos@imperial.ac.uk
2   Faculty of Engineering, Environment and Computing, Coventry University, Priory Street,
    Coventry CV1 5FB, UK
*   Correspondence: n.kuganathan@imperial.ac.uk

Abstract: Carbon nanotubes are of great interest for their ability to functionalize with atoms for adsorbing toxic gases such as CO, NO, and NO₂. Here, we use density functional theory in conjunction with dispersion correction to examine the encapsulation and adsorption efficacy of SO₂ and H₂S molecules by a (14,0) carbon nanotube and its substitutionally doped form with Ru. Exoergic encapsulation and adsorption energies are calculated for pristine nanotubes. The interaction of molecules with pristine nanotube is non-covalent as confirmed by the negligible charge transfer. The substitutional doping of Ru does not improve the encapsulation significantly. Nevertheless, there is an important enhancement in the adsorption of molecules by Ru-doped (14,0) nanotube. Such strong adsorption is confirmed by the strong chemical interaction between the nanotube and molecules. The promising feature of Ru-doped nanotubes can be tested experimentally for SO₂ and H₂S gas sensing.

Keywords: SWNT; sensor; DFT; encapsulation; charge transfer

1. Introduction

Single walled nanotubes (SWNTs) have attracted great interest due to their promising mechanical, chemical, and thermal properties and high surface area [1–5]. In recent years, there have been several experimental and theoretical studies showing the potential applications of SWNTs [6–12]. Applications include the use of SWNTs in energy storage and energy conversion devices [13,14], high-strength composites [15–17], nanoprobes and sensors [18–20], actuators [21,22], electronic devices [23,24], catalysis [25,26], and hydrogen storage media [27,28].

SWNTs are promising candidate materials to detect harmful gaseous molecules at low concentration [29–31]. Such detection is crucial to monitor environmental pollution. Many experimental and theoretical studies show that low concentration of small gaseous molecules such as NO₂, NH₃, NO, CO₂, and CH₄ can be trapped by SWNTs [32–35].

Modification of the surface of SWNTs via metal doping has been shown to be an efficient strategy to improve the adsorption of gaseous molecules [36–39]. A variety of transition metal doped SWNTs have been modelled theoretically to increase the efficacy of NH₃ and NO₂ molecules [36–41]. Though there are many studies focusing on the capture of nitrogen-containing pollutants by metal-doped nanotubes, a few studies have considered the adsorption of sulfur-containing pollutants. Sulfur-containing pollutants are also important to consider for removal as they can damage agriculture, aquatic life, and building structures. Numerous theoretical simulations have considered the interaction of SO₂ and H₂S with pristine SWNTs and concluded that the interaction between the nanotube and SO₂ and H₂S molecules are weak [42–44]. Metal doped SWNTs have also been considered theoretically to enhance the interaction of those molecules [45,46]. Zhang et al. [47] used density functional theory (DFT) simulation to study the adsorption of SO₂

and H$_2$S molecules on the Au-doped SWNT. Atom functionalized carbon nanotubes have been recently considered by Liao et al. [48] for H$_2$S sensing and splitting.

In this study, we use spin-polarized mode of DFT simulations together with dispersion to study the encapsulation and adsorption of SO$_2$ and H$_2$S gases with pristine and Ru-doped SWNT. Simulations enabled the calculation of the encapsulation/adsorption energies, charge transfer, and the electronic nature of the resultant composites relative to that of pristine SWNT.

2. Computational Methods

The spin-polarized DFT code VASP (Vienna Ab initio simulation package) was used to perform all calculations [49,50]. The generalized gradient approximation (GGA) parameterized by Perdew, Burke, and Ernzerhof (PBE) was applied to model the exchange-correlation term [51]. The valence electronic configurations for C, S, O, and H were 2s^2 2p^2, 3s^2 3p^4, 2s^2 2p^4, and 1s^1 respectively. A plane-wave basis set with a cut-off of 500 eV and the standard projected augmented wave (PAW) potentials [52] as implemented in the VASP code were used. A 2 × 2 × 1 Monk-horst Pack [53] k-point mesh was used to model pristine SWNT and molecules encapsulated or adsorbed-SWNT structures. For calculations on the molecules encapsulated or adsorbed-SWNT, periodic boundary conditions were applied to enforce a minimum lateral separation of 30 Å between structures in adjacent unit cells. In all cases the dimension of the cell was 30 Å × 30 Å ×17.28 Å. The number of atoms in the simulation box for all configurations are provided in the electronic Supplementary Information (see Table S1).

A conjugate gradient algorithm [54] was used to optimize the structures. The Hellman-Feynman theorem with Pulay corrections was used to obtain the forces on the atoms. Forces on the atoms in all optimized configurations were smaller than 0.04 eV/Å. The van-der Waals interaction was included in the form of semi-empirical pair-wise force field as implemented by Grimme et al. [55]. The Bader charge analysis [56,57] was carried out to calculate the charge transferred between the nanotube and the molecules. Initial magnetic moments for all atoms were set to one (e.g., MAGMOM = 227*1 for SO$_2$@SWNT, which has 227 atoms in total).

The encapsulation energy of SO$_2$ molecule was calculated by considering the difference in the total energy of the SO$_2$@SWNT and the total energies calculated for an isolated SO$_2$ molecule and an isolated SWNT.

$$E_{enc} = E_{(SO2@SWNT)} - E_{SWNT} - E_{SO2} \tag{1}$$

where E$_{(SO2@SWNT)}$ is the total energy of SO$_2$ encapsulated within a SWNT; E$_{SWNT}$ and E$_{SO2}$ are the total energies of a SWNT and an isolated gas phase SO$_2$ molecule. Similar equations were used to calculate the encapsulation energies of H$_2$S and adsorption energies of SO$_2$ and H$_2$S.

3. Results

3.1. Encapsulation of SO$_2$ and H$_2$S within SWNT

The encapsulation of SO$_2$ and H$_2$S molecules was first considered within SWNT. In all cases we used a (14,0) semiconducting nanotube. Figure 1 shows the relaxed configurations and charge density plots showing the interactions between the nanotube and the molecules. Optimized configurations in different orientations are provided in the electronic Supplementary Information (see Figure S1). Both SO$_2$ and H$_2$S molecules occupy the center of the nanotube. The encapsulation energies calculated for SO$_2$ and H$_2$S are −0.27 eV and −0.20 eV, respectively (see Table 1). This indicates that both molecules are energetically stable inside the nanotube compared to their isolated gaseous forms. The interaction between the molecules and the nanotube is non-covalent. This is further confirmed by the charge density plots (see Figure 1c,d), a very small charge transfer from the nanotube to the molecules and almost zero magnetic moments as calculated for the pristine nanotube. The calculated density of states (DOS) plot shows that (14,0) nanotube is a semiconductor

(band gap = 0.4 eV). DOS plots calculated for encapsulated and adsorbed complexes are not significantly affected (see Figure 1c–e).
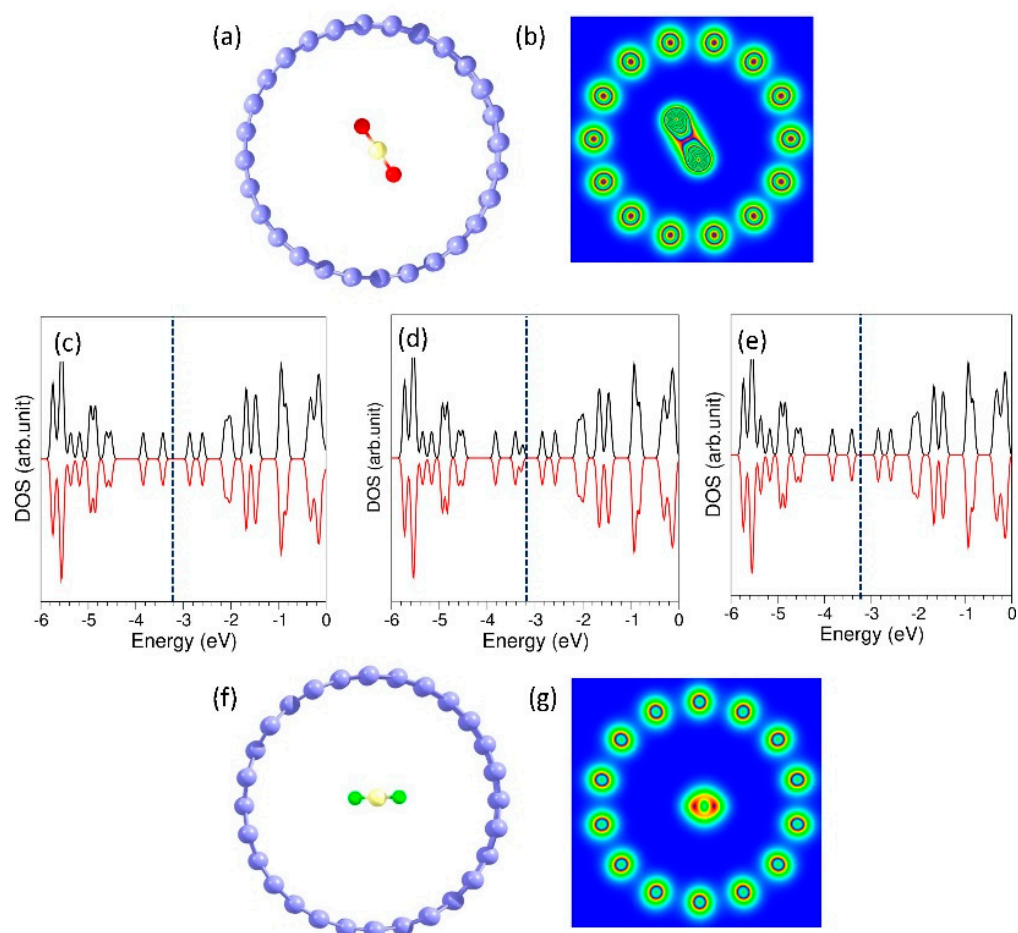

Figure 1. (**a**) Relaxed structure of a single SO_2 molecule encapsulated within SWNT, (**b**) charge density plot showing the interaction of SO_2 molecule with nanotube, (**c**) DOS plot of a pristine SWNT, (**d**) DOS plot of SO_2@SWNT, (**e**) DOS plot of H_2S@SWNT, (**f**) relaxed structure of a H_2S molecule inside the nanotube, and (**g**) its charge density plot. Vertical dashed lines correspond to the Fermi level.

Table 1. Calculated encapsulation energies with respect to molecules, the amount of charge transferred between the nanotube and the molecule, and net magnetic moments of the pristine nanotube and the encapsulated complexes.

System	Encapsulation Energy (eV)	Charge Transfer	Magnetic Moment
SWNT	—	—	0.00
SO_2@SWNT	−0.27	0.11	0.10
H_2S@SWNT	−0.20	0.02	0.00

3.2. Adsorption of SO_2 and H_2S on the Surface of SWNT

Next, we considered the adsorption of SO_2 and H_2S molecules on the surface of SWNT. The optimized configurations and charge densities showing the interaction of molecules with the SWNT are shown in Figure 2. Optimized configurations in different orientations are provided in the electronic Supplementary Information (see Figure S2). Adsorption is exoergic for both SO_2 and H_2S molecules meaning that the SWNT is capable of adsorbing

these molecules on the surface (see Table 2). Both relaxed structures and charge density plots show that the interaction with the surface is weak. The adsorption energy calculated for SO_2 molecule is slightly more negative than that calculated for H_2S molecule. The weak adsorption is further confirmed by the negligible charge transfer and zero magnetic moments. The Fermi levels calculated of the complexes are not altered significantly and retain the semiconducting character of the SWNT (band gap = 0.4 eV).
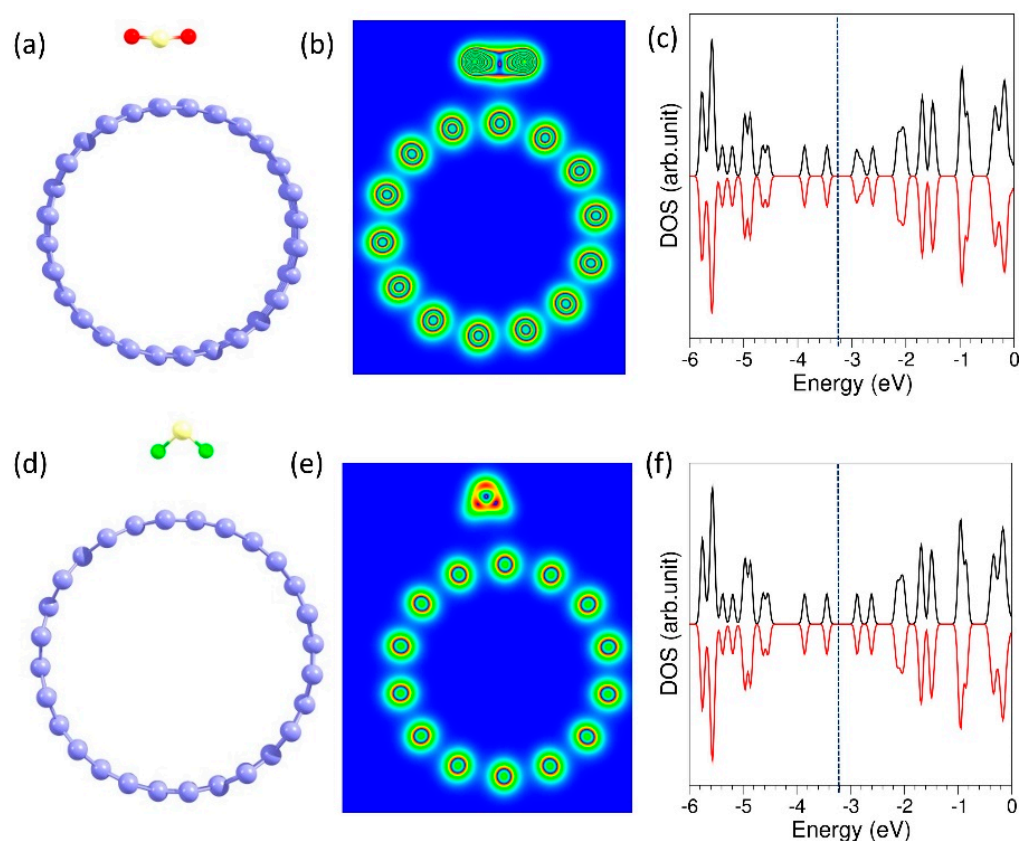

Figure 2. (**a**) Relaxed structure of a single SO_2 molecule adsorbed on the surface of SWNT, (**b**) charge density plot showing the interaction of SO_2 molecule with the nanotube, (**c**) DOS plot of SO_2-adsorbed nanotube, (**d**) relaxed structure of H_2S molecule adsorbed on the surface of the nanotube, (**e**) its charge density plot, and (**f**) DOS plot of H_2S-adsorbed nanotube. Vertical dashed lines correspond to the Fermi level.

Table 2. Calculated adsorption energies with respect to molecules, the amount of charge transferred between the nanotube and the molecule, and net magnetic moments of pristine nanotube and the adsorbed complexes.

System	Adsorption Energy (eV)	Charge Transfer	Magnetic Moment
SWNT	—	—	0.00
SO_2_SWNT	−0.23	0.09	0.00
H_2S_SWNT	−0.15	0.01	0.00

3.3. Ru-Doped SWNT

Aiming to improve the encapsulation or adsorption efficacy, a single Ru atom was substitutionally doped on the surface of SWNT. The relaxed configuration together with bond distances and Bader charges are shown in Figure 3. The doped Ru atom is in a trigonal pyramid configuration with an outward displacement (see Figure 3a). The Ru-C bond distances are longer than the C-C bond distances (see Figure 3b). The bonding interaction

between the Ru atom and the nanotube is further confirmed by the charge density plot (see Figure 3c). The Bader charge on the Ru atom is calculated to be +1.01, meaning that ~one electron has been donated by the Ru atom to the nearest neighbor C atoms (see Figure 3d). This is partly due to the larger electronegativity of C (2.55) than that of the Ru atom (2.20) [58]. The doping of the Ru atom significantly affects the DOS plot with some Ru states appearing near the Fermi level (see Figure 3e), leading to narrow-gap semiconductor (band gap = 0.1 eV). This is further confirmed by the atomic DOS plot of Ru (see Figure 3f).
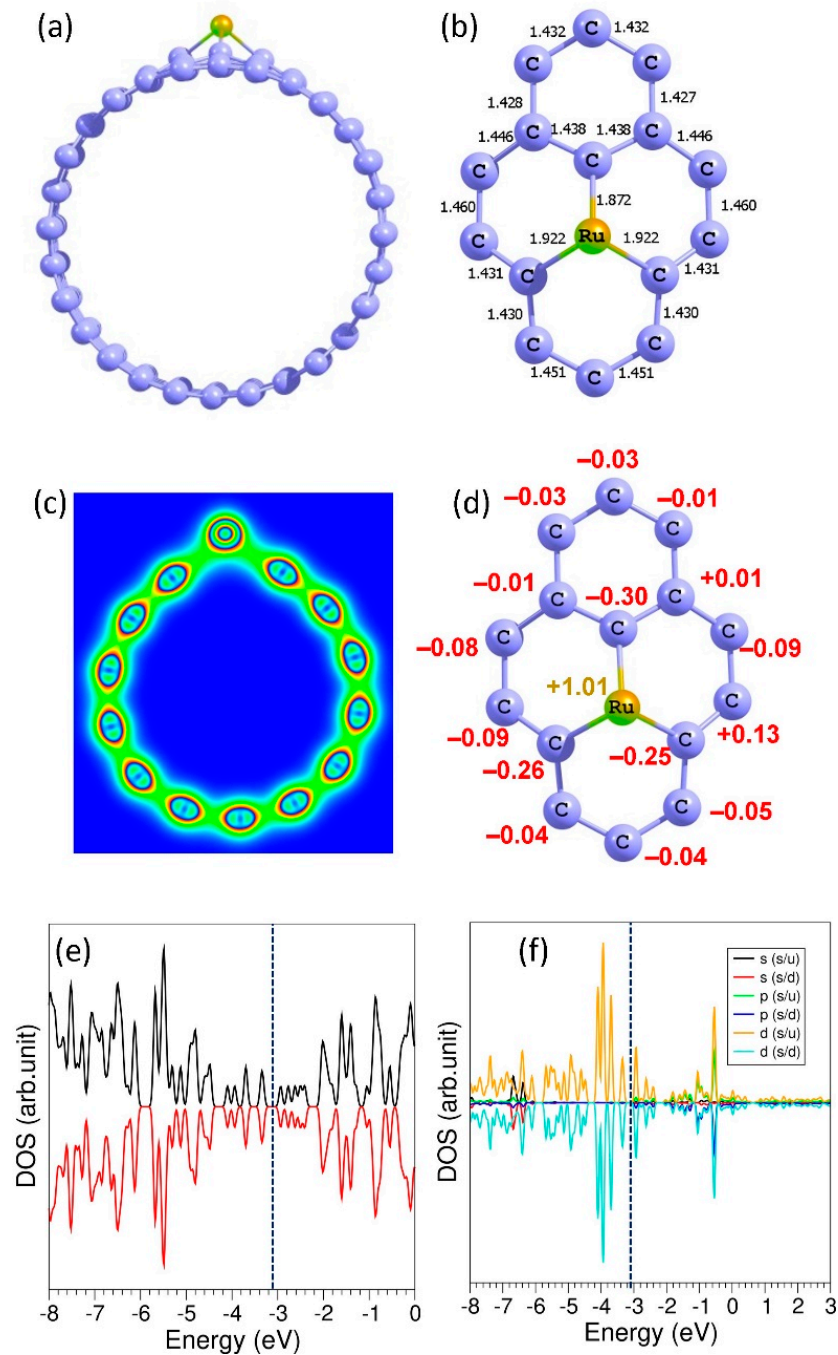

Figure 3. (**a**) Relaxed configuration of the Ru-doped SWNT, (**b**) calculated bond distances measured in Ångström around the defect, (**c**) charge density plot showing the interaction between the Ru atom and the nanotube, (**d**) Bader charge on the Ru atom and the nearest neighbor C atoms, and (**e**) total DOS plot and (**f**) the atomic DOS plot calculated for the Ru atom. Vertical dashed lines correspond to the Fermi level.

3.4. Encapsulation of SO$_2$ and H$_2$S within Ru-Doped SWNT

Next, the molecules were allowed to encapsulate with Ru-doped SWNT. The relaxed structures, charge density plots, and DOS plots are shown in Figure 4. Optimized configurations in different orientations are provided in the electronic Supplementary Information (see Figure S3). Table 3 reports the encapsulation energies, charge transferred between the nanotube and the molecules, and the net magnetic moments of the complexes. Encapsulation is exoergic for both SO$_2$ and H$_2$S molecules. There is a slight enhancement in the encapsulation energies. However, they are still non-covalent. This is consistent with the encapsulated structures and charge density plots (see Figure 3). The charge transfer is minimal in both cases though there is a slight increase in the charge transfer for the encapsulation of SO$_2$. The SWNT encapsulated with SO$_2$ exhibits a small magnetic moment of 0.30. The net magnetic moment of the SWNT encapsulated with H$_2$S is zero. The total DOS plot shows that the SWNT encapsulated with SO$_2$ is semi-metallic while the SWNT encapsulated with H$_2$S is a narrow gap semiconductor (see Figure 4c,d).
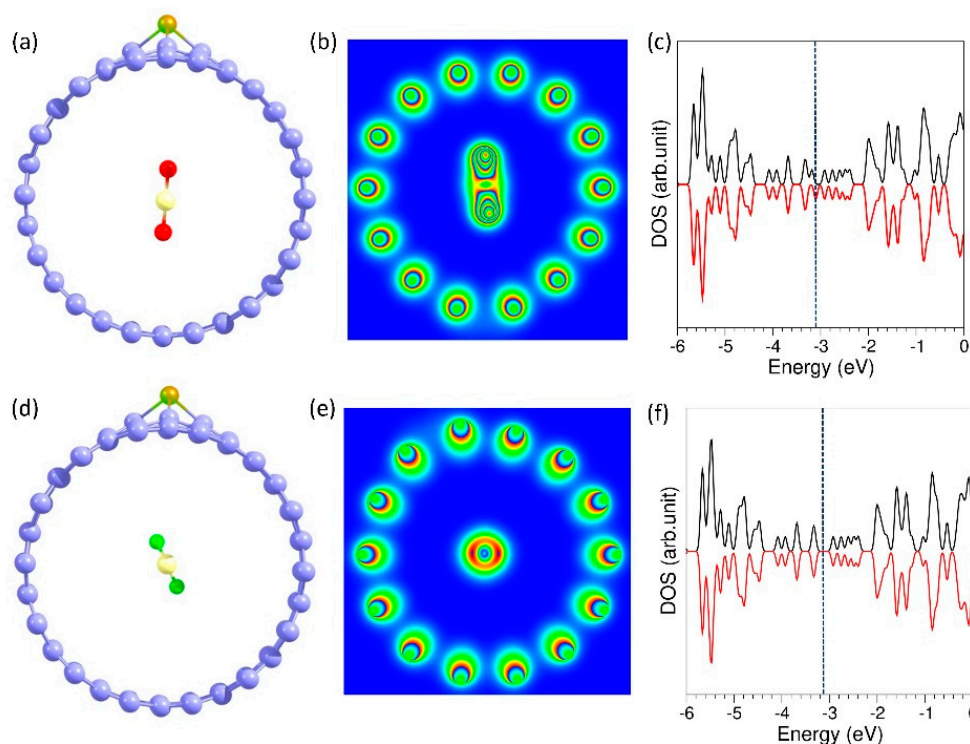

Figure 4. (**a**) Relaxed structure of a single SO$_2$ molecule encapsulated within the Ru-doped SWNT, (**b**) charge density plot showing the interaction of SO$_2$ molecule with the nanotube, and (**c**) the total DOS plot of the encapsulated configuration. Similar plots are shown for H$_2$S encapsulated SWNT (**d**–**f**). Vertical dashed lines correspond to the Fermi level.

Table 3. Calculated encapsulated energies with respect to molecules, the amount of charge transferred between the nanotube and the molecule and net magnetic moments of pristine nanotube and the adsorbed complexes.

System	Encapsulation Energy (eV)	Charge Transfer	Magnetic Moment
SWNT	—	—	0.00
SO$_2$@Ru.SWNT	−0.29	0.11	0.30
H$_2$S@Ru.SWNT	−0.23	0.02	0.00

3.5. Adsorption of SO₂ and H₂S on the Surface of Ru-Doped SWNT

Finally, we considered the adsorption of molecules on the surface of Ru-doped SWNT. Figure 5 shows the relaxed structure of the SO_2 adsorbed on the surface of Ru-doped SWNT together with the charge density plot and the total DOS plot. Optimized configurations in different orientations are provided in the electronic Supplementary Information (see Figure S4). The SO_2 molecule is chemically bonded via one of its oxygen atoms with the Ru atom, forming a Ru-O chemical bond (see Figure 5a,b). The Ru-O bond distance is calculated to be 2.171 Å. Adsorption is significantly enhanced upon doping. The calculated adsorption energy is -1.08 eV stronger by 0.85 eV than that calculated for the pure surface of the SWNT (see Table 4). The stronger adsorption is further confirmed by the charge density plot (see Figure 5c) and the significant charge transfer (0.52 e) from SWNT to the SO_2 molecule. The total density plot shows that the resultant complex is metallic (refer Figure 5d). The magnetic moment of 0.67 implies that the resultant complex is magnetic.
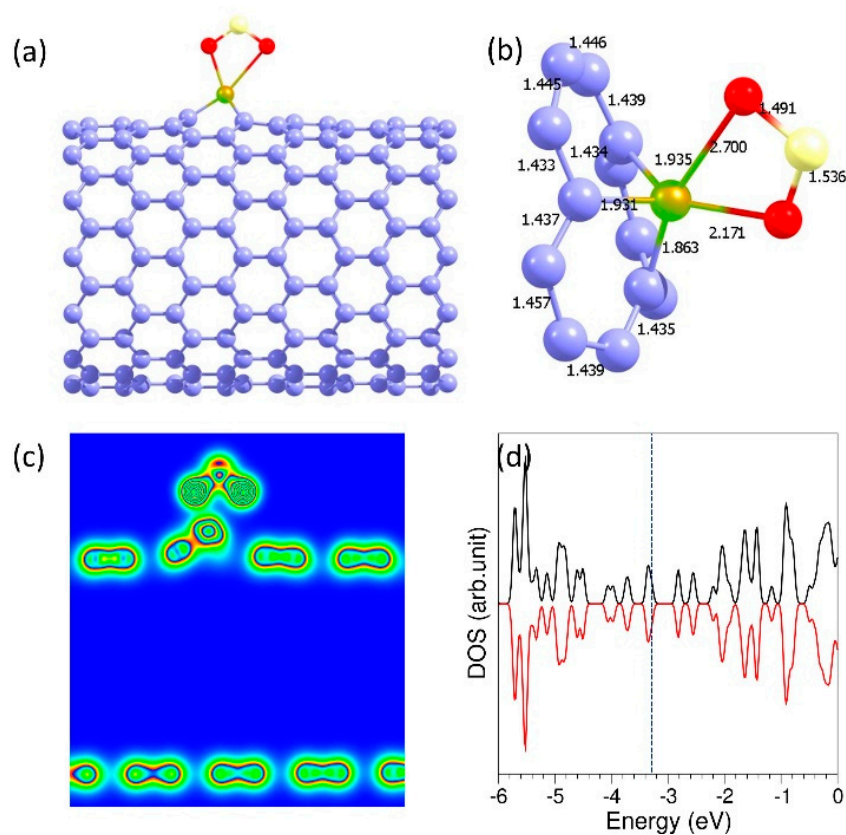

Figure 5. (**a**) Relaxed structure of a single SO_2 molecule adsorbed on the surface of Ru-doped SWNT, (**b**) side view of the relaxed configuration showing the Ru-C and Ru-O bond distances measured in Angström, (**c**) charge density plot showing the interaction of SO_2 molecule with the nanotube, and (**d**) the total DOS plot of the adsorbed configuration. Vertical dashed lines correspond to the Fermi level.

Table 4. Calculated adsorption energies with respect to molecules, the amount of charge transferred between the nanotube and the molecule, and net magnetic moments of pristine nanotube and the adsorbed complexes.

System	Adsorption Energy (eV)	Charge Transfer	Magnetic Moment
SWNT	—	—	0.00
SO₂_Ru.SWNT	−1.08	0.52	0.67
H₂S_Ru.SWNT	−1.00	0.07	0.00

In the case of H_2S molecule, there is a strong chemical interaction between the Ru atom and the S atoms in H_2S (see Figure 6). This is also confirmed by the bonding interaction between the Ru atom and the S atoms. The Ru-S bond length is calculated to be 2.463 Å slightly longer than the Ru-O bond observed in the interaction of SO_2 with Ru-adsorbed SWNT. The calculated adsorption energy is −1.00 eV meaning that the doping enhanced the adsorption by 0.85 eV. The strong adsorption is evidenced by the charge density plot. The Bader charge analysis shows that a small amount of charge is transferred from the nanotube to the H_2S molecule. The calculated DOS plot shows that the resultant complex retains its semiconducting character (band gap = 0.4 eV) though there is a dispersion in the valence and conduction bands by Ru states.
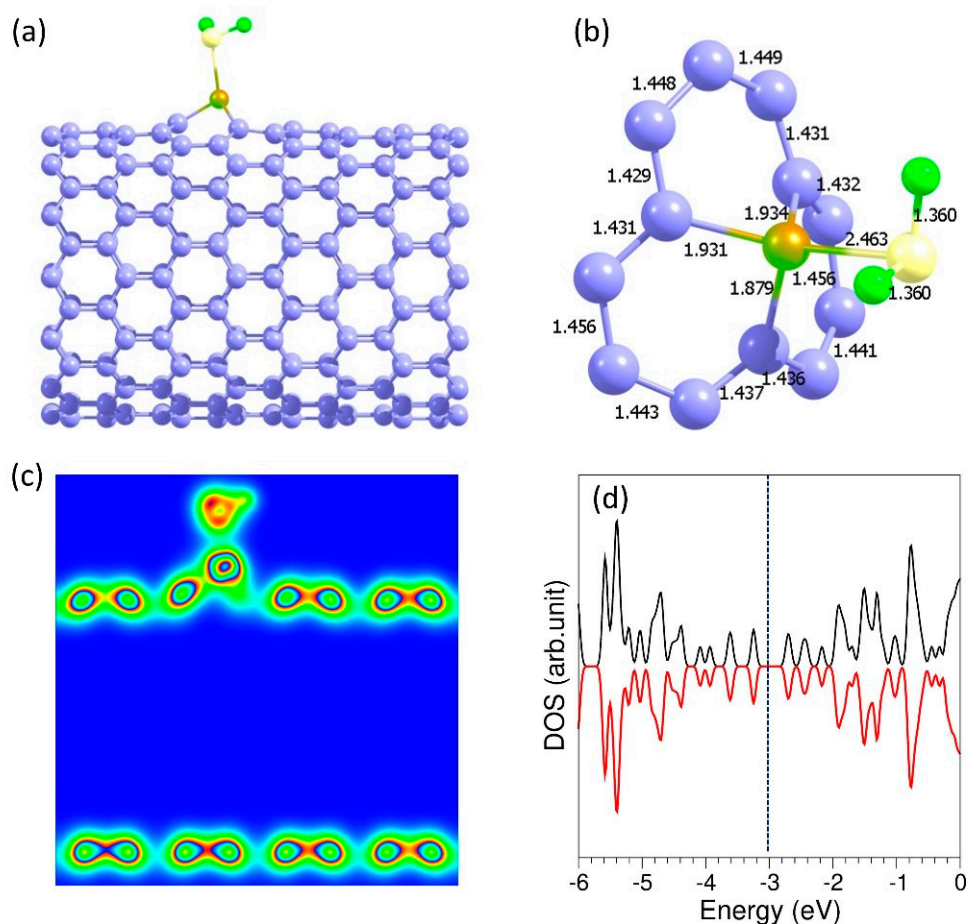

Figure 6. (**a**) Relaxed structure of a single H_2S molecule adsorbed on the surface of Ru-doped SWNT, (**b**) side view of the relaxed configuration showing the Ru-C and Ru-S bond distances measured in Angström, (**c**) charge density plot showing the interaction of H_2S molecule with the nanotube, and (**d**) the total DOS plot of the adsorbed configuration. Vertical dashed lines correspond to the Fermi level.

4. Conclusions

Carbon nanotubes provide a high inner and outer surface area to trap SO_2 and H_2S molecules. The efficacy of adsorption can be improved by modifying the surface of nanotube. Spin-polarized DFT simulations together with dispersion correction were employed to examine the encapsulation and adsorption efficacy of SO_2 and H_2S molecules by a pristine (14,0) SWNT and Ru-doped SWNT. Both SO_2 and H_2S were encapsulated and adsorbed exothermically but non-covalently by pristine SWNT, suggesting that molecules are more stable on the surface than their isolated gaseous forms. The doping of the Ru atom improved the encapsulation very slightly. However, strong adsorption is found for both molecules by the Ru-doped SWNT. Such strong adsorption is confirmed by the chemical

interaction between the S or O atom on the guest molecule side and the Ru atom on the nanotube side. To conclude, SWNT and its doped form with the Ru atom are shown to encapsulate and adsorb both SO_2 and H_2S molecules. The promising feature of Ru-doped SWNT for the significant adsorption of gases should be verified experimentally.

Supplementary Materials: The following are available online at https://www.mdpi.com/article/10.3390/chemosensors9060120/s1, Figure S1: Optimized configurations of SWNT encapsulated by (a) SO_2 molecule and (b) H_2S molecule, Figure S2: Optimized configurations of SWNT adsorbed by (a) SO_2 molecule and (b) H_2S molecule, Figure S3: Optimized configurations of Ru-doped SWNT encapsulated by (a) SO_2 molecule and (b) H_2S molecule, Figure S4: Optimized configurations of Ru-doped SWNT adsorbed by (a) SO_2 molecule and (b) H_2S molecule, Table S1: Number atoms in a SO_2 and H_2S molecule encapsulated within SWNST or adsorbed on the SWNT.

Author Contributions: Computation, N.K.; writing, N.K.; analysis and editing, N.K., writing—original draft preparation, N.K.; writing—review and editing, A.C. Both authors have read and agreed to the published version of the manuscript.

Institutional Review Board Statement: Not applicable.

Informed Consent Statement: Not applicable.

Data Availability Statement: Not applicable.

Conflicts of Interest: The author declares no conflict of interest.

References

1. Rao, R.; Pint, C.L.; Islam, A.E.; Weatherup, R.S.; Hofmann, S.; Meshot, E.R.; Wu, F.; Zhou, C.; Dee, N.; Amama, P.B.; et al. Carbon Nanotubes and Related Nanomaterials: Critical Advances and Challenges for Synthesis toward Mainstream Commercial Applications. *ACS Nano* **2018**, *12*, 11756–11784. [CrossRef] [PubMed]
2. Popov, V.N. Carbon nanotubes: Properties and application. *Mater. Sci. Eng. R Rep.* **2004**, *43*, 61–102. [CrossRef]
3. Gupta, N.; Gupta, S.M.; Sharma, S.K. Carbon nanotubes: Synthesis, properties and engineering applications. *Carbon Lett.* **2019**, *29*, 419–447. [CrossRef]
4. Chen, Y.-R.; Weng, C.-I.; Sun, S.-J. Electronic properties of zigzag and armchair carbon nanotubes under uniaxial strain. *J. Appl. Phys.* **2008**, *104*, 114310. [CrossRef]
5. Yazdani, H.; Hatami, K.; Eftekhari, M. Mechanical properties of single-walled carbon nanotubes: A comprehensive molecular dynamics study. *Mater. Res. Express* **2017**, *4*, 055015. [CrossRef]
6. Calatayud, D.G.; Ge, H.; Kuganathan, N.; Mirabello, V.; Jacobs, R.M.J.; Rees, N.H.; Stoppiello, C.T.; Khlobystov, A.N.; Tyrrell, R.M.; Como, E.D.; et al. Encapsulation of Cadmium Selenide Nanocrystals in Biocompatible Nanotubes: DFT Calculations, X-ray Diffraction Investigations, and Confocal Fluorescence Imaging. *ChemistryOpen* **2018**, *7*, 144–158. [CrossRef]
7. Hu, Z.; Pantoş, G.D.; Kuganathan, N.; Arrowsmith, R.L.; Jacobs, R.M.J.; Kociok-Köhn, G.; O'Byrne, J.; Jurkschat, K.; Burgos, P.; Tyrrell, R.M.; et al. Interactions Between Amino Acid-Tagged Naphthalenediimide and Single Walled Carbon Nanotubes for the Design and Construction of New Bioimaging Probes. *Adv. Funct. Mater.* **2012**, *22*, 503–518. [CrossRef]
8. Mao, B.; Calatayud, D.G.; Mirabello, V.; Kuganathan, N.; Ge, H.; Jacobs, R.M.J.; Shepherd, A.M.; Martins, J.A.R.; De La Serna, J.B.; Hodges, B.J.; et al. Fluorescence-Lifetime Imaging and Super-Resolution Microscopies Shed Light on the Directed- and Self-Assembly of Functional Porphyrins onto Carbon Nanotubes and Flat Surfaces. *Chemistry* **2017**, *23*, 9772–9789. [CrossRef]
9. Bekyarova, E.; Ni, Y.; Malarkey, E.B.; Montana, V.; McWilliams, J.L.; Haddon, R.C.; Parpura, V. Applications of Carbon Nanotubes in Biotechnology and Biomedicine. *J. Biomed. Nanotechnol.* **2005**, *1*, 3–17. [CrossRef]
10. Hofferber, E.M.; Stapleton, J.A.; Iverson, N.M. Review—Single Walled Carbon Nanotubes as Optical Sensors for Biological Applications. *J. Electrochem. Soc.* **2020**, *167*, 037530. [CrossRef]
11. Venkataraman, A.; Amadi, E.V.; Chen, Y.; Papadopoulos, C. Carbon Nanotube Assembly and Integration for Applications. *Nanoscale Res. Lett.* **2019**, *14*, 220. [CrossRef] [PubMed]
12. He, H.; Pham-Huy, L.A.; Dramou, P.; Xiao, D.; Zuo, P.; Pham-Huy, C. Carbon Nanotubes: Applications in Pharmacy and Medicine. *Biomed Res. Int.* **2013**, *2013*, 578290. [CrossRef]
13. Dillon, A.C. Carbon Nanotubes for Photoconversion and Electrical Energy Storage. *Chem. Rev.* **2010**, *110*, 6856–6872. [CrossRef] [PubMed]
14. Sun, L.; Wang, X.; Wang, Y.; Zhang, Q. Roles of carbon nanotubes in novel energy storage devices. *Carbon* **2017**, *122*, 462–474. [CrossRef]
15. Wu, A.S.; Chou, T.-W. Carbon nanotube fibers for advanced composites. *Mater. Today* **2012**, *15*, 302–310. [CrossRef]

16. Sharma, S.P.; Lakkad, S.C. Effect of CNTs growth on carbon fibers on the tensile strength of CNTs grown carbon fiber-reinforced polymer matrix composites. *Composites Part A Appl. Sci. Manuf.* **2011**, *42*, 8–15. [CrossRef]

17. Yadav, M.D.; Dasgupta, K.; Patwardhan, A.W.; Joshi, J.B. High Performance Fibers from Carbon Nanotubes: Synthesis, Characterization, and Applications in Composites—A Review. *Ind. Eng. Chem. Res.* **2017**, *56*, 12407–12437. [CrossRef]

18. Norizan, M.N.; Moklis, M.H.; Ngah Demon, S.Z.; Halim, N.A.; Samsuri, A.; Mohamad, I.S.; Knight, V.F.; Abdullah, N. Carbon nanotubes: Functionalisation and their application in chemical sensors. *RSC Adv.* **2020**, *10*, 43704–43732. [CrossRef]

19. Manzetti, S.; Vasilache, D.; Francesco, E. Emerging carbon-based nanosensor devices: Structures, functions and applications. *Adv. Manuf.* **2015**, *3*, 63–72. [CrossRef]

20. Dai, H.; Hafner, J.H.; Rinzler, A.G.; Colbert, D.T.; Smalley, R.E. Nanotubes as nanoprobes in scanning probe microscopy. *Nature* **1996**, *384*, 147–150. [CrossRef]

21. Baughman, R.H.; Cui, C.; Zakhidov, A.A.; Iqbal, Z.; Barisci, J.N.; Spinks, G.M.; Wallace, G.G.; Mazzoldi, A.; De Rossi, D.; Rinzler, A.G.; et al. Carbon Nanotube Actuators. *Science* **1999**, *284*, 1340–1344. [CrossRef] [PubMed]

22. Li, C.; Thostenson, E.T.; Chou, T.-W. Sensors and actuators based on carbon nanotubes and their composites: A review. *Compos. Sci. Technol.* **2008**, *68*, 1227–1249. [CrossRef]

23. Peng, L.-M.; Zhang, Z.; Wang, S. Carbon nanotube electronics: Recent advances. *Mater. Today* **2014**, *17*, 433–442. [CrossRef]

24. Cao, Y.; Cong, S.; Cao, X.; Wu, F.; Liu, Q.; Amer, M.R.; Zhou, C. Review of Electronics Based on Single-Walled Carbon Nanotubes. *Top. Curr. Chem.* **2017**, *375*, 75. [CrossRef] [PubMed]

25. Melchionna, M.; Marchesan, S.; Prato, M.; Fornasiero, P. Carbon nanotubes and catalysis: The many facets of a successful marriage. *Catal. Sci. Tech.* **2015**, *5*, 3859–3875. [CrossRef]

26. Esteves, L.M.; Oliveira, H.A.; Passos, F.B. Carbon nanotubes as catalyst support in chemical vapor deposition reaction: A review. *J. Ind. Eng. Chem.* **2018**, *65*, 1–12. [CrossRef]

27. Froudakis, G.E. Hydrogen storage in nanotubes and nanostructures. *Mater. Today* **2011**, *14*, 324–328. [CrossRef]

28. Mohan, M.; Sharma, V.K.; Kumar, E.A.; Gayathri, V. Hydrogen storage in carbon materials—A review. *Energy Storage* **2019**, *1*, e35. [CrossRef]

29. Zhang, W.-D.; Zhang, W.-H. Carbon Nanotubes as Active Components for Gas Sensors. *J. Sens.* **2009**, *2009*, 160698. [CrossRef]

30. Brahim, S.; Colbern, S.; Gump, R.; Grigorian, L. Tailoring gas sensing properties of carbon nanotubes. *J. Appl. Phys.* **2008**, *104*, 024502. [CrossRef]

31. Tang, R.; Shi, Y.; Hou, Z.; Wei, L. Carbon Nanotube-Based Chemiresistive Sensors. *Sensors* **2017**, *17*, 882. [CrossRef] [PubMed]

32. Panes-Ruiz, L.A.; Shaygan, M.; Fu, Y.; Liu, Y.; Khavrus, V.; Oswald, S.; Gemming, T.; Baraban, L.; Bezugly, V.; Cuniberti, G. Toward Highly Sensitive and Energy Efficient Ammonia Gas Detection with Modified Single-Walled Carbon Nanotubes at Room Temperature. *ACS Sensors* **2018**, *3*, 79–86. [CrossRef]

33. Ellison, M.D.; Crotty, M.J.; Koh, D.; Spray, R.L.; Tate, K.E. Adsorption of NH_3 and NO_2 on Single-Walled Carbon Nanotubes. *J. Phys. Chem. B* **2004**, *108*, 7938–7943. [CrossRef]

34. Yang, Y.; Narayanan Nair, A.K.; Sun, S. Adsorption and Diffusion of Carbon Dioxide, Methane, and Their Mixture in Carbon Nanotubes in the Presence of Water. *J. Phys. Chem. C* **2020**, *124*, 16478–16487. [CrossRef]

35. Bagherinia, M.A.; Shadman, M. Investigations of CO_2, CH_4 and N_2 physisorption in single-walled silicon carbon nanotubes using GCMC simulation. *Int. Nano Lett.* **2014**, *4*, 95. [CrossRef]

36. Yeung, C.S.; Liu, L.V.; Wang, Y.A. Adsorption of Small Gas Molecules onto Pt-Doped Single-Walled Carbon Nanotubes. *J. Phys. Chem. C* **2008**, *112*, 7401–7411. [CrossRef]

37. Sharafeldin, I.M.; Allam, N.K. DFT insights into the electronic properties and adsorption of NO_2 on metal-doped carbon nanotubes for gas sensing applications. *New J. Chem.* **2017**, *41*, 14936–14944. [CrossRef]

38. Yeung, C.S.; Chen, Y.K.; Wang, Y.A. Theoretical Studies of Substitutionally Doped Single-Walled Nanotubes. *J. Nanotechnol.* **2010**, *2010*, 801789. [CrossRef]

39. Abdullah, H.Y. Theoretical study of the binding energy of some gases on Al-doped carbon nanotube. *Results Phys.* **2016**, *6*, 1146–1151. [CrossRef]

40. Azizi, K.; Karimpanah, M. Computational study of Al- or P-doped single-walled carbon nanotubes as NH_3 and NO_2 sensors. *Appl. Surf. Sci.* **2013**, *285*, 102–109. [CrossRef]

41. Zhang, J.; Yang, G.; Tian, J.; Ma, D.; Wang, Y. First-principles study on the gas sensing property of the Ge, As, and Br doped $PtSe_2$. *Mater. Res. Express* **2018**, *5*, 035037. [CrossRef]

42. Oftadeh, M.; Gholamian, M.; Abdallah, H.H. Sulfur Dioxide Internal and External Adsorption on the Single-Walled Carbon Nanotubes: DFT Study. *Phys. Chem. Res.* **2014**, *2*, 30–40.

43. Oftadeh, M.; Gholamian, M.; Abdallah, H.H. Investigation of interaction hydrogen sulfide with (5,0) and (5,5) single-wall carbon nanotubes by density functional theory method. *Int. Nano Lett.* **2013**, *3*, 7. [CrossRef]

44. Babaheydari, A.K.; Jafari, A.; Moghadam, G.; Tavakoli, K. Investigation and Study of Adsorption Properties of H_2S on Carbon Nanotube (8, 0) (SWCNT) Using Density Functional Theory Calculation. *Adv. Sci. Lett.* **2013**, *19*, 3201–3205. [CrossRef]

45. An, L.; Jia, X.; Liu, Y. Adsorption of SO_2 molecules on Fe-doped carbon nanotubes: The first principles study. *Adsorption* **2019**, *25*, 217–224. [CrossRef]

46. Guo, G.; Wang, F.; Sun, H.; Zhang, D. Reactivity of silicon-doped carbon nanotubes toward small gaseous molecules in the atmosphere. *Int. J. Quantum Chem.* **2008**, *108*, 203–209. [CrossRef]

47. Zhang, X.; Dai, Z.; Chen, Q.; Tang, J. A DFT study of SO$_2$ and H$_2$S gas adsorption on Au-doped single-walled carbon nanotubes. *Phys. Scr.* **2014**, *89*, 065803. [CrossRef]
48. Liao, T.; Kou, L.; Du, A.; Chen, L.; Cao, C.; Sun, Z. H$_2$S Sensing and Splitting on Atom-Functionalized Carbon Nanotubes: A Theoretical Study. *Adv. Theory Simul.* **2018**, *1*, 1700033. [CrossRef]
49. Kresse, G.; Hafner, J. Ab initio molecular dynamics for liquid metals. *Phys. Rev. B* **1993**, *47*, 558–561. [CrossRef] [PubMed]
50. Kresse, G.; Furthmüller, J. Efficient iterative schemes for ab initio totaCambridgel-energy calculations using a plane-wave basis set. *Phys. Rev. B* **1996**, *54*, 11169–11186. [CrossRef]
51. Perdew, J.P.; Burke, K.; Ernzerhof, M. Generalized Gradient Approximation Made Simple. *Phys. Rev. Lett.* **1996**, *77*, 3865–3868. [CrossRef] [PubMed]
52. Blöchl, P.E. Projector augmented-wave method. *Phys. Rev. B* **1994**, *50*, 17953–17979. [CrossRef]
53. Monkhorst, H.J.; Pack, J.D. Special points for Brillouin-zone integrations. *Phys. Rev. B* **1976**, *13*, 5188–5192. [CrossRef]
54. Press, W.H.; Teukolsky, S.A.; Vetterling, W.T.; Flannery, B.P. *Numerical Recipes in C: The Art of Scientific Computing*, 2nd ed.; Cambridge University Press: Cambridge, UK, 1992.
55. Grimme, S.; Antony, J.; Ehrlich, S.; Krieg, H. A consistent and accurate ab initio parametrization of density functional dispersion correction (DFT-D) for the 94 elements H-Pu. *J. Chem. Phys.* **2010**, *132*, 154104. [CrossRef] [PubMed]
56. Bader, R.F.W. The zero-flux surface and the topological and quantum definitions of an atom in a molecule. *Theor. Chem. Acc.* **2001**, *105*, 276–283. [CrossRef]
57. Henkelman, G.; Arnaldsson, A.; Jónsson, H. A fast and robust algorithm for Bader decomposition of charge density. *Comput. Mater. Sci.* **2006**, *36*, 354–360. [CrossRef]
58. Lide, D.R. *CRC Handbook of Chemistry and Physics*, 86th ed.; CRC: Boca Raton, FL, USA, 2005.